Long-term incubations provide insight into the mechanisms of anaerobic oxidation of methane in methanogenic lake sediments

Hanni Vigderovich[a], Werner Eckert[b], Michal Elul[a], Maxim Rubin-Blum[c], Marcus Elvert [d], Orit Sivan[a]

[a] Department of Earth and Environmental Science, Ben-Gurion University of the Negev, Beer Sheva, Israel

[b] Israel Oceanographic & Limnological Research, The Yigal Allon Kinneret Limnological Laboratory, Israel

[c] Israel Oceanographic & Limnological Research, Haifa, Israel

[d] MARUM - Center for Marine Environmental Sciences and Faculty of Geosciences, University of Bremen, Bremen, Germany

Corresponding author: Hanni Vigderovich, hannil@post.bgu.ac.il

Abstract

Anaerobic oxidation of methane (AOM) is one of the major processes limiting the release of the greenhouse gas methane from natural environments. In Lake Kinneret (Israel), geochemical profiles and experiments with fresh sediments indicate that iron-coupled AOM (Fe-AOM) sequesters 10-15% of the methane produced in the methanogenic zone (>20 cm sediment depth). The oxidation of methane in this environment was shown to be mediated by a combination of *mcr* gene-bearing archaea and aerobic bacterial methanotrophs. Here, we aimed to investigate the AOM process in terms of various electron acceptors and involved microorganisms during long-term anaerobic sediment slurry incubations (~ 18 months) under controlled conditions. We followed the process with the addition of ^{13}C-labeled methane and two stages of incubations: (i) enrichment of the microbial population involved in AOM and (ii) slurry dilution and manipulations, including addition of multiple electron acceptors (metal oxides, nitrate, nitrite and humic substances) and inhibitors for methanogenesis/AOM and sulfate reduction. Carbon isotope measurements in the dissolved inorganic pool in these long-term incubations suggest that considerable AOM consumed 3-8% of the methane produced at a rate of 2.0±0.4 nmol gr^{-1} dry sediment day^{-1}. Carbon isotope measurements in lipids and metagenomic analyses indicate that only anaerobic microbes catalyzed this AOM. Whereas cryptic oxidation of methane by combining archaea and aerobic methanotrophs is feasible in the natural Lake Kinneret sediments, reverse methanogenesis dominates methane turnover in the long-term controlled experiments. Humic substances and iron oxides, but not sulfate, manganese, nitrate, and nitrite, are the likely electron acceptors used during the AOM. Our observations support the contrast between methane oxidation mechanisms in naturally anoxic lake sediments, with potentially co-existing aerobes and anaerobes, and long-term incubations, where anaerobes prevail.

Keywords: Anaerobic oxidation of methane (AOM), lake, sediments, dissolved inorganic carbon, stable isotopes, electron acceptor, methanotrophs

1. Introduction

Methane (CH_4) is an effective greenhouse gas (Wuebbles and Hayhoe, 2002) with anthropogenic and natural sources. Natural methane sources contribute about 50% of this gas emission to the atmosphere (Saunois et al., 2020). Aerobic and anaerobic oxidation of methane (AOM) naturally control the release of this gas to the atmosphere (Conrad, 2009; Reeburgh, 2007; Knittel and Boetius, 2009). While sulfate-dependent AOM, catalyzed by ANaerobic MEthanotrophs (ANMEs) 1-3, is widespread mostly in marine sediments (Hoehler et al., 1994; Boetius et al., 2000; Orphan et al., 2001; Treude et al., 2005, 2014), in other environments methane oxidation can be coupled to other electron acceptors.

AOM coupled to the reduction of iron and manganese oxides has been confirmed in several environments (Beal et al., 2009; Egger et al., 2015; Sivan et al., 2011; Sivan et al., 2014; Segarra et al., 2013; Bar-or et al., 2017; Aromokeye et al., 2020; Su et al., 2020; Mostovaya et al., 2021). Alternative electron acceptors for AOM include other metals, humic substances, nitrate and nitrite. The synthetic analog for humic substances, 9,10-anthraquinone-2,6-disulfonate (AQDS), was shown to serve as a terminal electron acceptor (Scheller et al., 2016; Valenzuela et al., 2017; Bai et al., 2019; Zhang et al., 2019; Fan et al., 2020). Nitrate-dependent AOM has been demonstrated in a consortium of archaea and denitrifying bacteria (Raghoebarsing et al., 2006) and in an enrichment culture of ANME-2d (Haroon et al., 2013; Arshad et al., 2015), whereas nitrite fuels AOM by *Methylomirabilis* (NC-10, Ettwig et al., 2010). ANME-2d and *Methylomirabilis* can also couple AOM to selenite reduction (Luo et al., 2018). The ubiquitous aerobic methanotrophs Methylococcales may oxidize methane and denitrify under hypoxia (Kits et al., 2015), switch to iron reduction (Zheng et al., 2020), or generate oxygen by methanobactins (Dershwitz et al., 2021). The latter study also showed the ability of alphaproteobacterial methanotroph *Methylocystis* sp. strain SB2 to couple methane oxidation and iron reduction.

In Lake Kinneret sediments, *in-situ* pore water profiles (Sivan et al., 2011), diagenetic models (Adler et al., 2011) and incubation experiments with fresh sediment slurries (Bar-Or et al., 2017) suggest that iron reduction coupled to AOM (Fe-AOM) removes 10-15% of the produced methane in the deep methanogenic zone (>20 cm below water-sediment interface). Analysis of the microbial community structure revealed that both methanogenic archaea and methanotrophic bacteria are potentially involved in methane oxidation (Bar-Or et al., 2015). Analyses of stable isotopes in fatty acids, the 16S rRNA gene amplicons and metagenomics showed that reverse methanogenesis by archaea and the bacterial type I aerobic methanotrophy by Methylococcales play a role in methane cycling (Bar-Or et al., 2017; Elul et al., 2021). This aerobic methanotrophic activity has been observed in several anoxic hypolimnions and sediments of lakes (Beck et al., 2013; Oswald et al., 2016; Martinez-Cruz et al., 2017; Cabrol et al., 2020), and might be fueled by the presence of oxygen at microlevel up to several meters below the oxycline. However, whether these methanotrophs continue to oxidize methane under strictly anoxic conditions and which electron acceptors are available is still unknown.

Here, we used long-term anaerobic incubations to assess the dynamics of methane-oxidizing microbes under anoxic conditions and to quantify various electron acceptors' availability for AOM. For this purpose, we diluted fresh methanogenic sediments from Lake Kinneret with original porewater from the same depth and amended the sediment with ^{13}C-labeled methane, following its oxidation to dissolved inorganic carbon (DIC). Our experiment design consisted of two stages, the first stage included the enrichment of the microbial population involved in AOM, and the second stage involved an additional slurry dilution and several manipulations with multiple electron acceptors and inhibitors. The potential electron acceptors were iron and manganese oxides, nitrate, nitrite and humic substances. We inhibited the *mcr* gene with 2-bromoethanesulfonate (BES), methanogens with acetylene and sulfate reduction and sulfur disproportionation with Na-Molybdate (Nollet et al., 1997; Orembland & Capone, 1988; Lovley & Klug, 1983). We measured methane oxidation rates (by the ^{13}C-DIC enrichment), the electron acceptor characteristics (by their addition or inhibition) and the evaluated changes in microbial diversity over various incubation periods (based on metagenomics and lipid biomarkers). The results from the long-term anaerobic incubations were compared to those of batch and semi-bioreactor experiments that were set up with fresh sediments to follow the changes in methane oxidation mechanisms.

2. Methods

2.1 Study site

Lake Kinneret (Sea of Galilee) is a warm monomictic freshwater lake located in the North of Israel. The lake is 21 km long and 13 km wide. Its maximum depth is ~42 m at the lake center (station A, Figure S1) and the average depth is 24 m. The lake is thermally stratified from March to December, with the hypolimnion turning anoxic from April. Surface water temperatures range from 15 to 30 ℃, and the bottom water temperatures remain between 14-17 ℃ all year long. The lake sediments are composed mostly of carbonates (40-50%) and clays (20%; Hadas and Pinkas, 1995; Eckert, 2000). The total iron content in the top 40 cm of the sediments is ~3 wt % (Serruya, 1971; Eckert, 2000; Bar-Or et al., 2017). The sediment at the deep methanogenic zone used in this study (~20 cm sediment depth from the water-sediment interface at the lake's center) contains 50% carbonates, 30% clay and 7% iron (Table S1). The porewater's dissolved organic carbon (DOC) concentration increases with depth, ranging from ~6 mg C L^{-1} at the sediment-water interface to 17 mg C L^{-1} at 25 cm depth (Adler et al., 2011). Dissolved methane concentrations in the porewater increase sharply from the top sediments to more than 2 mM at 15 cm depth and then decrease to 0.5 mM (Adler et al., 2011; Sivan et al., 2011; Bar-Or et al., 2015).

2.2 Experimental set-up

This study compares three incubation strategies (A, B and C) of Lake Kinneret methanogenic sediments amended with original porewater from the same depth, ^{13}C-labeled methane, different potential electron

acceptors for AOM (nitrite, nitrate, metal oxides and humic substances) and inhibitors for sulfur cycling and methanogens' activity (Fig. 1):

A) Long-term two-stage slurry incubations with a first stage of 1:1 sediment to porewater ratio for three months with high methane content to enrich the microorganisms involved in the AOM. After three months, the slurry was diluted to a 1:3 ratio, then different reactants were added to the incubations, which were monitored for up to 18 months.

B) Semi-continuous bioreactor experiments with freshly collected sediments and porewater at a 1:4 ratio (respectively), where porewater was exchanged regularly.

C) Batch incubation experiments with fresh sampled sediments and porewater at a 1:5 ratio, respectively, and several manipulations (this experimental set-up was described in our previous studies (Bar-Or et al., 2017; Elul et al., 2021)).

Here below we describe the experiments. Detailed protocols are found in the supplementary information.

2.2.1 Experiment set-up A: Long-term two-stage incubations

The sediments for the slurries were collected during several sampling campaigns between 2017 and 2019 from the central lake (Station A, Fig. S1) using a gravity corer with 50 cm Perspex cores. Sediments from the methanogenic zone (> 20 cm depth) were diluted with porewater from the methanogenic zone of parallel cores sampled on the same day. The porewater was extracted by centrifugation at 9300 g for 15 minutes, filtered by 0.22 μM filters into 250 ml glass bottles, sealed with a rubber stopper, and flushed for 30 minutes with N_2.

In the first stage, the sediment was diluted with the extracted porewater to create a 1:1 ratio slurry in 250 ml glass bottles with a headspace of 70-90 ml under continuous N_2 flushing (Fig. 1). The slurries were flushed with N_2 (99.999%, MAXIMA, Israel) for 30 minutes. Methane was injected using a gas-tight syringe for a final content of 20% in the headspace, where 10% of the injected methane was ^{13}C-labeled methane (99%, Sigma-Aldrich). When significant AOM was observed by the increase of $\delta^{13}C_{DIC}$ after three months (Fig. S2), the incubations were either transferred to the second stage experiments or continued to run with porewater exchange and $\delta^{13}C_{DIC}$ values monitored every three months.

This study presents ten sets of two-stage incubation experiments with different treatments (electron acceptors/shuttling/inhibitors). They were all set up similarly (protocols in the supplementary information): subsamples (~18 g each) of the pre-incubation slurry were transferred with a syringe under continuous flushing of N_2 gas into 60 ml glass bottles and diluted with fresh anoxic porewater from the methanogenic zone (as described above) to achieve a 1:3 sediment to porewater ratio (Fig. 1), leaving 24 ml of headspace in each experiment bottle. The bottles were crimp-sealed, flushed with N_2

136 gas for 5 minutes, shaken vigorously and flushed again (3 times). ^{13}C-labeled methane was added to all
137 the bottles as described in Table 1. The "killed" control bottles in each experiment were autoclaved
138 twice, cooled, and only then were amended with the appropriate treatments and ^{13}C-labeled methane.

139 Electron acceptors were added either as a powder (hematite, magnetite, clay, MnO_2, humic substances)
140 or in dissolved form in double-distilled water (DDW) (KNO_3 and $NaNO_2$). The involvement of sulfur
141 cycling was tested by inhibition with Na-molybdate (Lovley and Klug, 1983), while the other electron
142 acceptors were tested for their potential participation by their addition to the slurries. AQDS was added
143 as an analog for humic substances, which was previously shown to serve as a terminal electron acceptor
144 for AOM and electron shuttling for iron reduction (e.g., Scheller et al., 2016; Sivan et al., 2016).
145 Amorphous iron ($Fe(OH)_3$) was prepared in the lab by dissolving $FeCl_3$ in DDW, then titrated with
146 NaOH 1.5 N up to pH 7 and was added to the bottles by injection. The final concentration of each
147 addition is detailed in Table 1. The ^{13}C-labeled methane was injected to all experiment bottles at the
148 beginning of each experiment (unless mentioned otherwise) using a gas-tight syringe from a stock bottle
149 filled with ^{13}C-labeled methane gas (which was replaced with saturated NaCl solution). Three different
150 inhibitors were added to three different experiments: molybdate, BES and acetylene. Molybdate was
151 added to experiment No. 1 to detect the feasibility of an active sulfur cycle. BES was added to
152 experiment No. 8 at the start of the experiment. Acetylene was added to experiment No. 9. It was
153 injected during the experiment to two bottles at different timepoints after ^{13}C enrichment in the DIC
154 was observed (Table 1).

155 All live treatments were set up in duplicates or triplicates and we present the average with an error bar.
156 In two experiments, only one "killed" control bottle was set up. The slurry was prioritized for other
157 treatments since the killed controls showed repetitive no activity for numerous previous experiments.
158 The humic substrate experiment used natural (humic) substance that were extracted from a different
159 lake. One experiment was set up without any additional electron acceptor to assess the rate of
160 methanogenesis in the two-stage slurries. Porewater was sampled anaerobically for $\delta^{13}C_{DIC}$ and
161 dissolved Fe(II) measurements in duplicates (2 ml), and methane was measured from the headspace.
162 Variations in the $\delta^{13}C_{DIC}$ values between the experiments resulted from different amounts of ^{13}C-labeled
163 methane injected at the start of each experiment.

164 2.2.2 Experiment set-up B: Semi-bioreactor

165 Semi-bioreactors regularly monitored the redox state at close-to-natural *in-situ* conditions for 15 months
166 in freshly collected sediments. Two 0.5 L semi-bioreactors (Fig. 1) (LENZ, Weinheim, Germany) were
167 set up with fresh sediments from the methanogenic zone (25 - 40 cm) of Lake Kinneret Station A
168 immediately after their collection. Both reactors were filled headspace-free with a slurry at a 1:4
169 sediment - pore water ratio. One of the bioreactors was amended with 10 mM hematite and the second
170 without it, serving as a control. To dissolve ^{13}C-labeled methane in the porewater, 15 ml of porewater

171 were replaced with 15 ml of methane gas (a mixture of $^{12}CH_4$ and $^{13}CH_4$) to produce methane-only
172 headspace for 24 hours. The reactors were shaken repeatedly during those hours. After 24 hours, the
173 gas was replaced with anoxic porewater, so that there was no headspace at all. This resulted in lower
174 methane concentrations than the batch experiments (0.2 mM vs. ~2 mM, respectively). Redox potential
175 was monitored continuously by electrode (Metrohm, Herisau, Switzerland) to verify anoxic conditions
176 and determine the redox state throughout the incubation period. The bioreactors were subsampled
177 weekly to bi-weekly, and the sample volume (5-10 ml) was replaced immediately by preconditioned
178 anoxic (flushed with N_2 gas for 15 minutes) porewater from the methanogenic zone. As outlined below,
179 samples were analyzed for dissolved Fe(II), CH_4, and $\delta^{13}C_{DIC}$. Additional subsamples for metagenome
180 and lipid analyses were taken at the beginning of the experiment and on days 151 and 382, respectively.

181 2.2.3 Experiment set-up C: Fresh batch experiment

182 Sediments for this experiment were collected in August 2013 at Station A, similar to the sediments for
183 the pre-incubations. The sediments below 26 cm depth were diluted under anaerobic conditions with
184 porewater from the same depth to reach a 1:5 sediment to porewater ratio. The slurry was divided into
185 60 ml experiment bottles with 40 ml slurry in each bottle. The sampling and experimental set-up details
186 are described in Bar-Or et al., 2017. Here we present the results of $\delta^{13}C_{DIC}$, metagenome and lipid
187 analyses of two treatments: natural (with only ^{13}C-labeled methane) and hematite. The experiment ran
188 for 15 months.

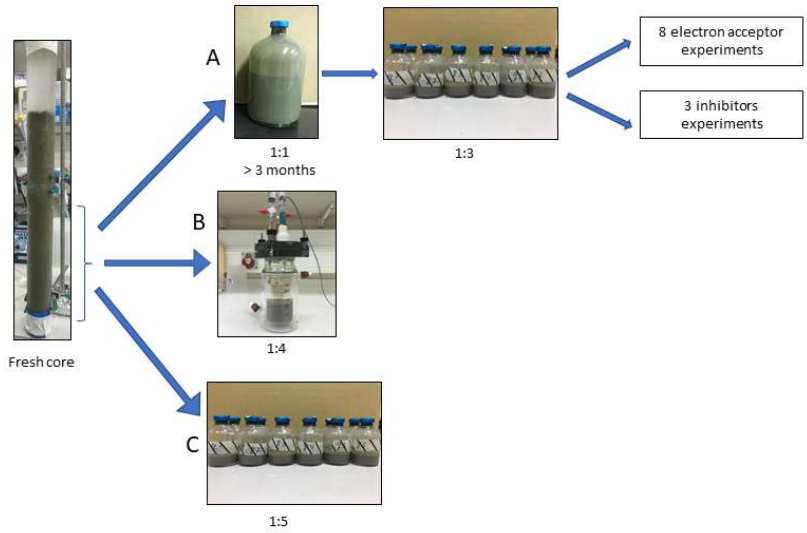

189

190 Figure 1: Flow diagram of the experimental design. Three types of experiments were set up from sediments of
191 the methanogenic zone (below 20 cm): A. Two-stage slurry experiments with diluted pre-incubated slurries and
192 porewater (1:3 sediment to porewater ratio). Ten experiments were set up this way, 8 of them with different
193 electron acceptors for 6-18 months, and three different inhibitors for 12-18 months (to one experiment, both
194 electron acceptors and an inhibitor were added). B. Semi-bioreactor experiment with freshly collected
195 sediments. C. Fresh batch experiment -slurry experiment with freshly collected sediments (Bar-Or et al., 2017).

196 Table 1: Specific details of the three types of experiments: two-stage, semi-bioreactor and fresh batch
197 experiments.

Experiment serial number (SN)	Experiment	Treament	# of bottles	CH_4 [ml]	$^{13}CH_4$ [ml]	Fe_2O_3 [mM]	Fe_3O_4 [mM]	$Fe(OH)_3$ [mM]	MnO_2 [mM]	NO_2^- [mM]	NO_3^- [mM]	AQDS [mM]	Humic substances [mM]	PCA [mM]	Fe-bearing montronite (clay) [gr]	Na_2-molybdate [mM]	BES [mM]	Acetylene [µL]	Temp [c°]	Duration [day]	Comments
1	Hematite	$^{13}CH_4$	2		1														20	201	
		$^{13}CH_4$+hematite	2		1	10													20		
2	Magnetite	$^{13}CH_4$	2		1											1			16	447	The methane that was added at the beginning of the experiment was not labelled, so ^{13}C-labeled methane was added after 105 days. Na_2-molybdate was added to one of the bottles on day 365
		$^{13}CH_4$+magnetite	2		1		10									1			16		Na_2-molybdate was added to one of the bottles on day 365
		$^{13}CH_4$+$Fe(OH)_3$	2		1			10								1			16		
		Killed+$^{13}CH_4$+magnetite	1		1		10												16		
3	MnO_2	$^{13}CH_4$	2		1.2														20	201	200 µL $^{13}CH_4$ was added on day 1, then another 1 mL was added on day 24.
		$^{13}CH_4$+MnO2	2		1.2				10										20		200 µL $^{13}CH_4$ was added on day 1, then another 1 mL was added on day 24.
4	Nitrate	$^{13}CH_4$+NO_3^- (high conc.)	2	1	0.5	12					1								20	306	
		$^{13}CH_4$+hematite	2	1	0.5	12													20		
		$^{13}CH_4$+NO_3^-(high conc.)+hematite	2	1	0.5	12					1								20		
		$^{13}CH_4$+NO_3^-(low conc.)+hematite	2	1	0.5	12					0.2								20		
		Killed+$^{13}CH_4$+NO_3^-(high conc.)+hematite	1	1	0.5	12					1								20		
5	Nitrite	$^{13}CH_4$	3	1	0.5														20	493	
		$^{13}CH_4$+NO_2^-(high conc.)+hematite	2	1	0.5	10				0.5									20		
		$^{13}CH_4$+NO_2^-(low conc.)+hematite	2	1	0.5	10				0.1									20		
		Killed+$^{13}CH_4$+NO_2^-(high conc.)+hematite	2	1	0.5	10				0.5									20		
6	AQDS	$^{13}CH_4$	3		1														20	264	
		$^{13}CH_4$+AQDS	2		1							5							20		
		$^{13}CH_4$+AQDS+hematite	2		1	10						5							20		
		Killed+$^{13}CH_4$+AQDS	2		1														20		
7	Natural humic acids and clay	$^{13}CH_4$	2		1	10													20	169	The head space of the experiment bottles was flushed with N_2 on day 51 and $^{13}CH_4$ was added. This was done in order to match the the clay bottles.
		$^{13}CH_4$+hematite	2		1	10													20		
		$^{13}CH_4$+humic acid	2		1								0.5						20		
		$^{13}CH_4$+clay	2		1	10									1				20		Clay was added on day 43, and the bottles were flushed again with N_2. $^{13}CH_4$ was added again on day 51.
		Killed+$^{13}CH_4$+hematite	2		1	10													20		
8	Bromoethanesulfonate (BES)	$^{13}CH_4$+hematite	2	9	1	10													20	493	
		$^{13}CH_4$+hematite+BES	2	9	1	10											20		20		
9	Acetylene	$^{13}CH_4$+hematite	4	1	0.5	10												120	20	321	Acetylene was injected to each bottle at different time point doring the experiment.
		$^{13}CH_4$+hematite+acetylene	2	1	0.5	10												120	20		
		Killed+$^{13}CH_4$+hematite	2	1	0.5	10													20		
10	No electron acceptor	No additions	3																20	147	
		$^{13}CH_4$	3		1														20		
	Semi-bioreactor	$^{13}CH_4$		15															16	345	
		$^{13}CH_4$+hematite		15		10													16	677	
	Freshly collected sediment exp.	$^{13}CH_4$			0.05														20	467	
		$^{13}CH_4$+hematite			0.05	20													20		

2.3 Analytical methods

Measurements of $\delta^{13}C_{DIC}$ were performed on a DeltaV Advantage Thermo Scientific isotope-ratio mass-spectrometer (IRMS). Results are reported referent to the Vienna Pee Dee Belemnite (VPDB) standard. For these measurements about 0.3 ml of filtered (0.22 µm) porewater was injected into a 12 ml glass vial with He atmosphere and 10 µl of H_3PO_4 85% to acidify all the DIC species to CO_2 (g). The headspace autosampler (CTC Analytics. Type PC PAL) took a gas sample from the vials and measured the $\delta^{13}C_{DIC}$ of the sample on the GasBench interface with a precision of ±0.1 ‰. DIC was measured on the IRMS using the peak height and a precision of 0.05 mM. Dissolved Fe(II) concentrations were measured using the ferrozine method (Stookey, 1970) by a spectrophotometer at 562 nm wavelength with a detection limit of 1 µmol L^{-1}. Methane concentrations were measured from the headspace. A 100 µL headspace sample was taken with a gas-tight syringe and was analyzed by a focus gas chromatograph (GC) equipped with a flame ionization detector (FID) with a detection limit of 0.005 µmol. Bottles to which acetylene was added were measured similarly for ethylene to determine the acetylene turnover with the N cycle.

A sub-set of samples (Table 3) was investigated for the assimilation of ^{13}C-labeled methane into polar lipid-derived fatty acids (PLFAs) and intact ether lipid-derived hydrocarbons. A total lipid extract (TLE) was obtained from 0.4 to 1.6 g of the freeze-dried sediment or incubated sediment slurry using a modified Bligh and Dyer protocol (Sturt et al., 2004). Before extraction, 1 µg of 1,2-diheneicosanoyl-*sn*-glycero-3-phosphocholine and 2-methyloctadecanoic acid were added as internal standards. PLFAs in the TLE were converted to fatty acid methyl esters (FAMEs) using saponification with KOH/MeOH and derivatization with BF_3/MeOH (Elvert et al., 2003). Intact archaeal ether lipids in the TLE were separated from the apolar archaeal lipid compounds using preparative liquid chromatography (Meador et al., 2014) followed by ether cleavage with BBr_3 in dichloromethane forming hydrocarbons (Lin et al., 2010). Both FAMEs and ether-cleaved hydrocarbons were analyzed by GC-mass spectrometry (GC-MS; Thermo Finnigan Trace GC coupled to a Trace MS) for identification and GC-IRMS (Thermo Scientific Trace GC coupled via a GC Isolink interface to a Delta V Plus) for determination of $\delta^{13}C$ values using the column and temperature program settings described by Aepfler et al. (2019). The $\delta^{13}C$ values are reported with an analytical precision better than 1‰ as determined by long-term measurements of an *n*-alkane standard with known isotopic composition of each compound. Reported fatty acid isotope data are corrected for the introduction of the methyl group during derivatization by mass balance calculation similar to equation 1 using the measured $\delta^{13}C$ value of each FAME and the known isotopic composition of methanol as input parameters.

For the metagenomic analyses, total genomic DNA was extracted from the semi-bioreactor experiment (duplicates a and b), pre-incubation slurries ($^{13}CH_4$-only control, $^{13}CH_4$ + hematite) and their respective initial slurries (t0), using the DNeasy PowerLyzer PowerSoil Kit (QIAGEN). Genomic DNA was eluted

using 50 µl of elution buffer and stored at −20°C. Metagenomics libraries were prepared at the sequencing core facility at the University of Illinois at Chicago using Nextera XT DNA library preparation kit (Illumina, USA). 19-40 million 2 × 150 bp paired-end reads per library were sequenced using Illumina NextSeq500. Metagenomes were co-assembled from concatenated reads of all metagenomic libraries with Spades V3.12 (Bankevich et al., 2012; Nurk et al., 2013), following decontamination, quality filtering (QV= 10) and adapter-trimming with the BBDuk tool from the BBMap suite (Bushnell B, http://sourceforge.net/projects/bbmap/). Downstream analyses, including reading coverage estimates, automatic binning with maxbin (Wu et al., 2014) and metabat2 (Kang et al., 2019) bin refining with DAS tool (Sieber et al., 2018), were performed within the SqueezeMeta framework (Tamames and Puente-Sánchez, 2019). GTDB-Tk was used to classify the metagenome-assembled genomes (MAGs) based on Genome Taxonomy Database release 95 (Parks et al., 2021). The principal component analysis biplot was constructed with Past V4.03 (Hammer et al., 2001).

Methanogenesis rate was calculated from temporal changes in methane concentration in a representative pre-incubated slurry experiment (Fig. S3). The amount of methane oxidized was calculated by a simple mass balance calculation according to equations 1 and 2:

$$x \times F^{13}CH_4 + (1 - x) \times FDI^{13}C_i = FDI^{13}C_f \quad (1)$$

$$[CH_4]_{ox} = x \times [DIC]_f \quad (2)$$

The final DIC pool comprises two end members; the initial DIC pool and the oxidized ^{13}C-CH_4. The term *x* denotes the fraction of oxidized ^{13}C-CH_4, while 1-*x* denotes the fraction of the initial DIC pool out of the final DIC pool. $F^{13}CH_4$ is the fraction of ^{13}C out of the total CH_4 at t0, $FDI^{13}C_i$ is the fraction of ^{13}C out of the total DIC at t0, and $FDI^{13}C_f$ is the fraction of ^{13}C out of the total DIC at t-final. $[CH_4]_{ox}$ is the amount (concentration in pore water) of the methane oxidized throughout the full incubation period, and $[DIC]_f$ is the DIC concentration at t-final. It was assumed that the isotopic composition of the labeled CH_4 did not change significantly throughout the incubation period.

3. Results

In ten sets of slurry incubation experiments, we followed the progress of the methane oxidation process in (type A) long-term two-stage incubations from Lake Kinneret methanogenic sediments (Figs. 2 and 3) by monitoring the changes $\delta^{13}C_{DIC}$ values, metagenomic and specific isotope lipid analyses. We also followed methane oxidation in a semi-bioreactor system (type B) with freshly collected sediments with or without the addition of hematite (Fig. 2). The results were compared to fresh batch slurry incubations (type C) from the same methanogenic zone, presented by Bar-Or et al. (2017) and Elul et al. (2021).

3.1 Geochemical trends in the two-stage experiments

In the two-stage experiments (type A), there was a conversion of ^{13}C-methane to ^{13}C-DIC in all the natural non-killed slurries, indicating significant AOM (Figs. 2 and 3). The $\delta^{13}C_{DIC}$ values of the natural sediment amended only with ^{13}C-methane treatments (the "methane-only" control) reached up to 743‰, even with the low abundance of microbial populations in these sediments. Average AOM rate in the methane-only controls was 2.0±0.4 nmol gr^{-1} dry sediment day^{-1} (Table 2). At the same time, methanogenesis occurred with a net methanogenesis rate of ~ 25 nmol gr dry sediment^{-1} day^{-1} (Fig. S3, Table S2, Table 2.). The two-stage geochemical experiments tested first the potential of several electron acceptors to perform and stimulate the AOM process, as detailed below.

3.1.1 Metals as electron acceptors

Iron and manganese oxides were added as potential electron acceptors. The addition of hematite to three different treatments increased the $\delta^{13}C_{DIC}$ values with time and reached up to 694‰ (Fig. 2), similarly to the natural (methane-only) controls. The average AOM rate in those treatments was 1.0±0.3 nmol gr dry sediment^{-1} day^{-1} (Table 2). Magnetite amendments resulted in a minor increase of $\delta^{13}C_{DIC}$ values compared to the methane-only controls (200‰ and 265‰, respectively, Fig. 3A) with an AOM rate of 1.8 nmol gr dry sediment^{-1} day^{-1}. Amorphous iron amendments resulted in only a 22‰ increase in $\delta^{13}C_{DIC}$ and a lower AOM rate (0.1 nmol gr dry sediment^{-1} day^{-1}, Fig. 3A and Table 2). The addition of iron-bearing clay nontronite did not cause any increase in the $\delta^{13}C_{DIC}$ values but dissolved Fe(II) concentrations increased compared to the natural methane-only control (Fig. 3B, Fig. 4). No AOM was detected 200 days following the addition of MnO_2 based on $\delta^{13}C_{DIC}$ estimates, whereas the $\delta^{13}C_{DIC}$ values of the methane-only controls reached over 500‰ (Fig. 3F).

3.1.2 Sulfate as an electron acceptor

The involvement of sulfate in the AOM of two-stage incubations was tested to detect the feasibility of an active cryptic sulfur cycle, even with the absence of detectable sulfate in the methanogenic sediments (Holmkvist et al., 2011). It was quantified directly by adding Na-molybdate, an inhibitor of sulfate reducers and sulfur disproportionators, to the methane-only controls and slurries amended with magnetite (Fig. 3A). This addition did not change the increase of $\delta^{13}C_{DIC}$ with time, and thus the AOM rates, similar to the observation in the fresh batch incubations (Bar-O et al., 2017).

3.1.3 Nitrate and nitrite as electron acceptors

Nitrate and nitrite involvement in the AOM was tested to detect the feasibility of an active cryptic nitrogen cycle, even with the absence of detectable nitrate and nitrite in the sediments. Nitrate was added at two different concentrations (0.2 and 1 mM, Fig. 3C) to the two-stage slurries amended with hematite, as these concentrations were shown previously to promote AOM in other settings (Ettwig et al., 2010). Hematite addition alone increased the $\delta^{13}C_{DIC}$ values by ~200‰ during the 306 days of the

298 experiment. The $\delta^{13}C_{DIC}$ in the bottles with the addition of 1 mM nitrate, with and without hematite
299 (Fig. 3C; the data points of the two treatments are on top of each other) decreased from 43‰ at the
300 beginning of the experiment to 35‰ after 306 days. The $\delta^{13}C_{DIC}$ in the bottles with the addition of 0.2
301 mM nitrate and hematite increased by 27‰ at the end of the experiment. We also observed no increase
302 in $\delta^{13}C_{DIC}$ during the first 222 days following the addition of 0.5 mM of nitrite (Fig. 3D), then $\delta^{13}C_{DIC}$
303 increased by 19‰ until the incubation was terminated. The respective AOM rate was 0.2 nmol gr dry
304 $sediment^{-1}$ day^{-1} (Table 2). Following the addition of 0.1 mM nitrite, $\delta^{13}C_{DIC}$ increased only after 130
305 days and reached 158‰ at day 493. The respective AOM rate was 0.5 nmol gr dry $sediment^{-1}$ day^{-1}. In
306 the methane-only controls, $\delta^{13}C_{DIC}$ value reached a maximum of 330‰.

307 3.1.4 Organic compounds as electron acceptors

308 Two of the two-stage incubation experiments were amended with synthetic and natural organic electron
309 acceptors to test the potential of organic electron acceptors. The addition of AQDS to slurries with and
310 without hematite decreased the $\delta^{13}C_{DIC}$ values during the entire experiment duration (Fig. 3E). The
311 dissolved Fe(II) showed an increase of 50 µM in these treatments, whereas without AQDS there was
312 an increase of 20 µM (Fig. S4). We further tested the effect of naturally occurring humic substances
313 using those isolated from a different natural lake. The results show that the $\delta^{13}C_{DIC}$ values did not change
314 at the beginning of the experiments (Fig. 3B), while a steep increase of ~90 µM in their Fe(II)
315 concentrations were observed (Fig. 4). After 20 days, the $\delta^{13}C_{DIC}$ values of these slurries started to
316 increase dramatically from 84‰ to 150‰ with an AOM rate of 1.2 nmol gr dry $sediment^{-1}$ day^{-1} (Fig.
317 3B, Table 2). We observed a mirrored trend of the dissolved Fe(II) concentrations to that of $\delta^{13}C_{DIC}$
318 with a steep increase during the first 20 days followed by a decrease of 37 µM (Fig. 4).

319 To evaluate which metabolic processes drive AOM, we analyzed $\delta^{13}C_{DIC}$ following the addition of
320 inhibitors: i) BES, a specific inhibitor for methanogens and ANME's *mcrA* genes and ii) acetylene, a
321 non-specific inhibitor for methanogens. Both cases showed complete inhibition of labeled ^{13}C-DIC
322 production following the addition, similarly to the killed control (Fig. 5). Acetylene can also inhibit
323 nitrogen cycling in some cases; however, this has been shown to result in the production of ethylene
324 (Oremland and Capone, 1988). In our case, no ethylene was detected, supporting the inhibition only of
325 methanogens' activity.

326

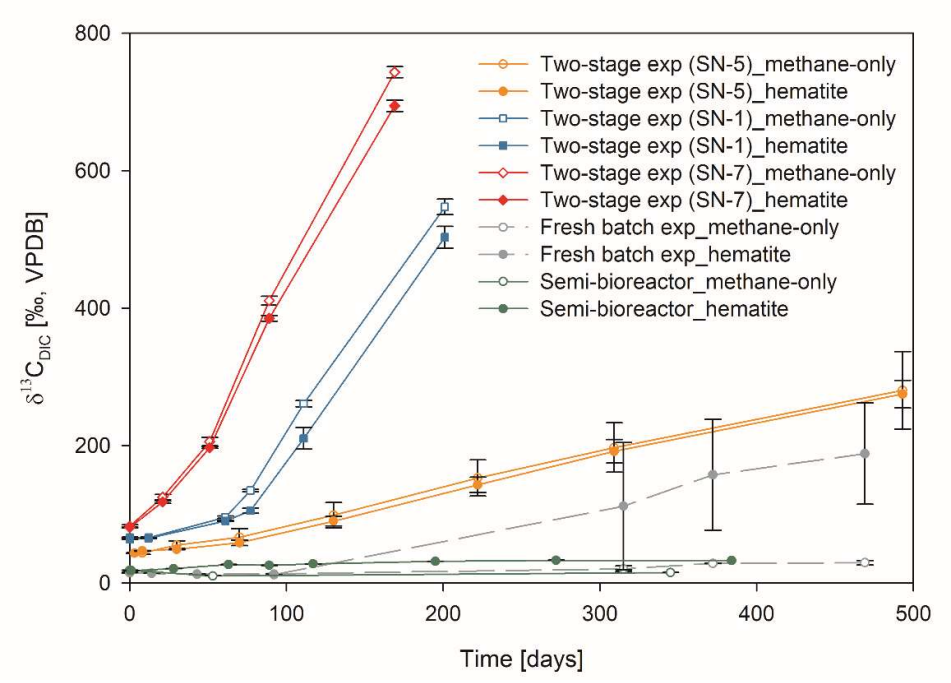

Figure 2: Comparison of $\delta^{13}C_{DIC}$ values among the three types of experiments: A) three two-stage slurry experiments; B) the semi-bioreactor experiment; and C) slurry batch experiment with freshly collected sediments (Bar-Or et al., 2017). In each experiment, two treatments are shown, with hematite (filled symbol) and without (empty symbols) hematite addition. The error bars represent the average deviation of the mean of duplicate/triplicate bottles.

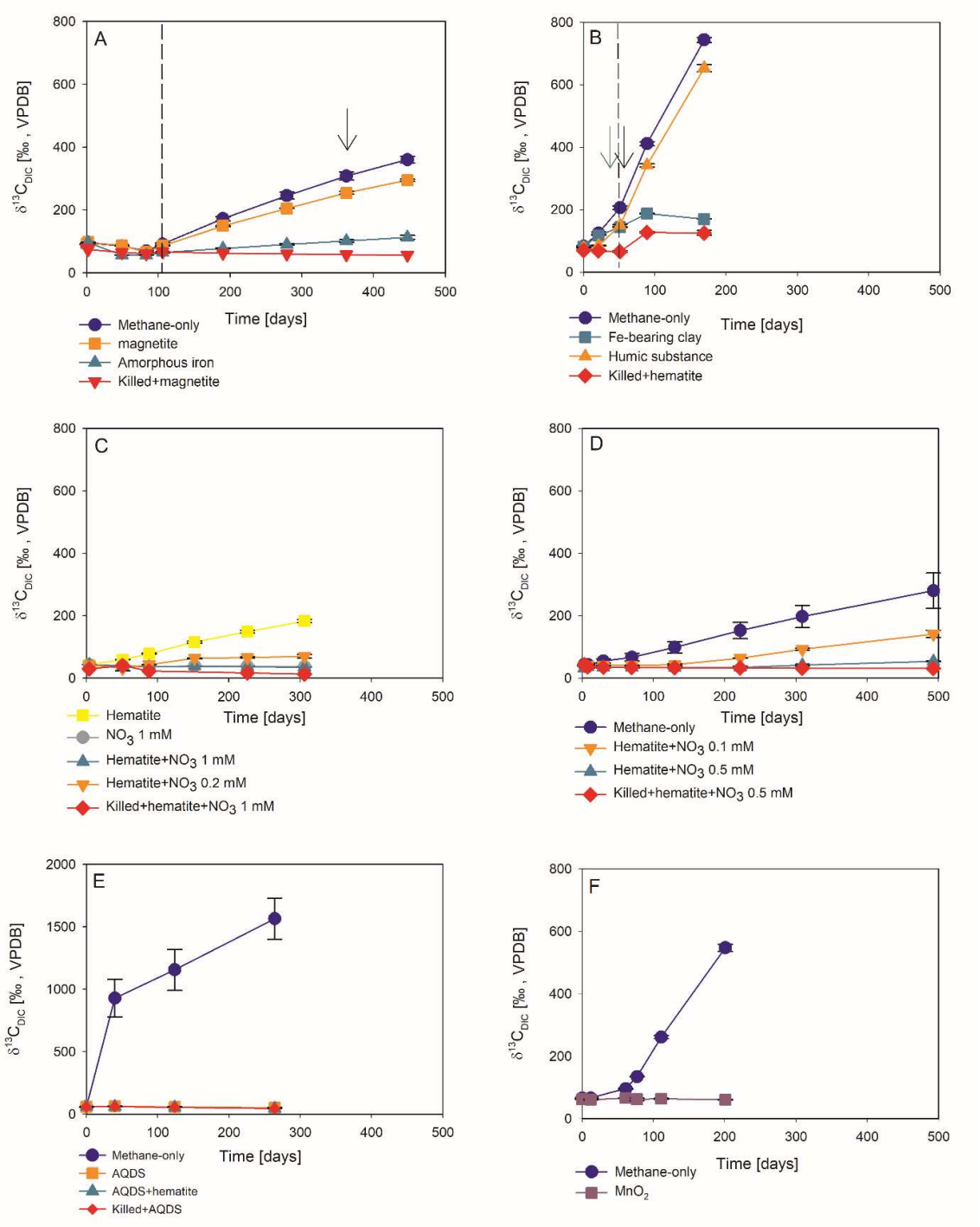

Figure 3: The potential of different electron acceptors for AOM in Lake Kinneret in the pre-incubated long-term slurry experiments with the following treatments: (A) with and without the addition of magnetite and amorphous iron ($Fe(OH)_3$). The dashed line represents the addition of ^{13}C -labeled CH_4. The black arrow represents the addition of Na-molybdate as an inhibitor for sulfate reduction. (B) with clay and natural humic substance. The green arrow represents the time clay was added to the relevant bottles, the dashed line represents the time the headspace of the bottles was flushed again with N_2, and the black arrow represents the second injection of 1 mL of ^{13}C -labeled methane. (C) with the addition of hematite and two different concentrations of nitrate. (D) with the

addition of hematite and two different concentrations of nitrite. (E) with the addition of AQDS. (F) with and without the addition of ^{13}C -labeled methane was added to all the bottles (specific details on each experiment can be found in Table 1). Error bars represent the average of the absolute deviations of data points from their mean.

Table 2: Methanogenesis and AOM rates in experiment A (two-stage slurries) amended with ^{13}C-labeled methane and different electron acceptors (methanogenesis rate was calculated in one of the experiments and was assumed to be similar in all of them).

Experiment serial number (SN)	Treatment	Methanogenesis rate [nmol/gr dry sediment X day]	AOM rate [nmol/gr dry sediment X day]	AOM/methanogenesis [%]
10	**methane only**	24.8	1.1	4.4
1	**methane only**	24.8	1.6	6.4
	methane+hematite	24.8	0.5	2.1
2	**methane only**	24.8	2.4	8.2
	methane+magnetite	24.8	1.8	6.3
	methane+amorphous iron	24.8	0.1	0.5
7	**methane only**	24.8	1.4	6.4
	methane+hematite	24.8	1.3	6.0
	methane+humics	24.8	1.2	5.4
5	**methane only**	24.8	1.0	4.6
	methane+hematite	24.8	1.0	4.6
	methane+hematite+nitrite 0.5 mM	24.8	0.2	0.8
	methane+hematite+nitrite 0.1 mM	24.8	0.5	2.1

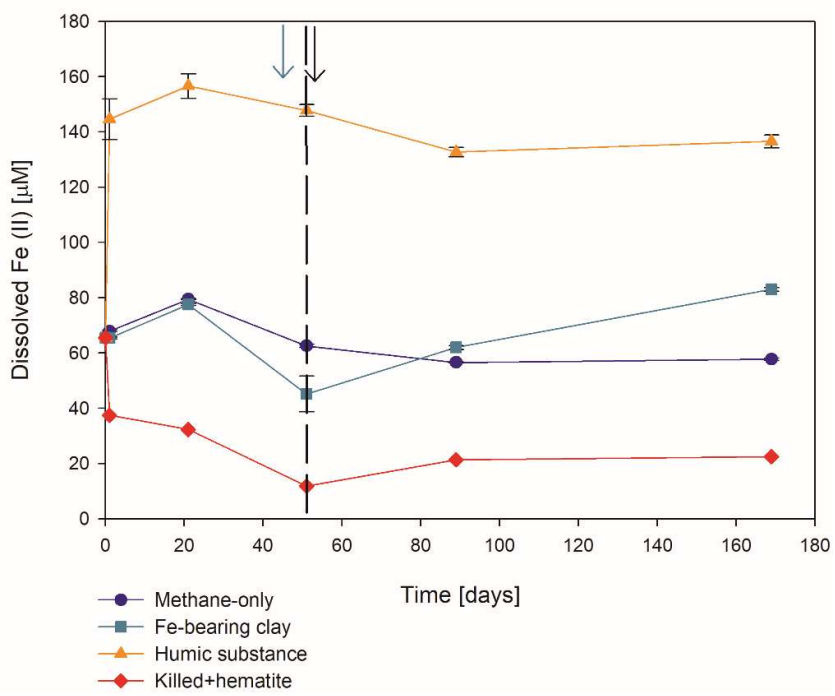

Figure 4: The dissolved Fe(II) change in the two-stage experiment No. 7 containing clay, natural humic acid, and PCA. The green arrow represents the time clay was added to the specific bottles and those bottles flushed with N_2, the dashed line represents the time the rest of the bottles were flushed, and the black arrow represents the time $^{13}CH_4$ was added again. Error bars represent the average of the absolute deviations of data points from their mean.

3.2 Microbial dynamics

Analyses of taxonomy and coverage of metagenome-assembled genomes suggest that in the pre-incubated slurries, Bathyarchaeia are the dominant archaea, together with putative methanogens such as Methanofastidiales (Thermococci), Methanoregulaceae (Methanomicrobia) and Methanotrichales (Methanosarcinia) (Supplementary coverage table). Bonafide ANME (ANME-1) were detected at substantial coverage of approximately 1 (the 27th most abundant out of 195 MAGs) in all the treatments. Among bacteria, sulfate reducers Desulfobacterota and Thermodesulfovibrionales (Nitrospirota) were prominent together with the GIF9 Dehalococcoida lineage, which is known to metabolize chlorinated compounds in lake sediments (Biderre-Petit et al., 2016). Some Methylomirabilales (NC10) were found (average coverage of 0.32±0.06), and no Methanoperedens were detected. Methylococcales methanotrophs were found in the natural sediments and fresh batch and bioreactor incubations (average of 0.34±0.02), as opposed to the average coverage of 0.09±0.04 in long-term incubations. Methylococcales comprised *Methyloterricola*, *Methylomonas* and *Methylobacter* genera (Supplementary coverage table). The methylotrophic partners of aerobic methanotrophs, *Methylotenera*, were found in fresh batch and bioreactor incubations, where *Methylomonas* was found, in line with previous studies showing their association (Beck et al., 2013). Principal component analysis

shows the grouping of long-term pre-incubated slurries, semi-bioreactor incubations, and fresh batch experiments (Fig. 6), emphasizing microbial dynamics over time.

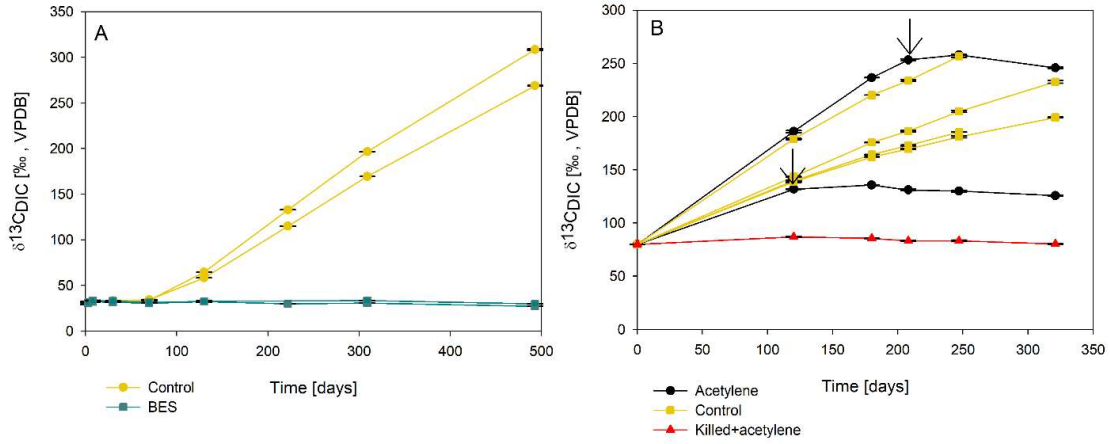

Figure 5: The change of $\delta^{13}C_{DIC}$ values with time in two long-term sediment slurry incubations amended with hematite and ^{13}C-labeled methane. (A) with/out BES and (B) with/out acetylene. Black arrows represent the time at which acetylene was injected to the experiment bottle. The error bars are smaller than the symbols.

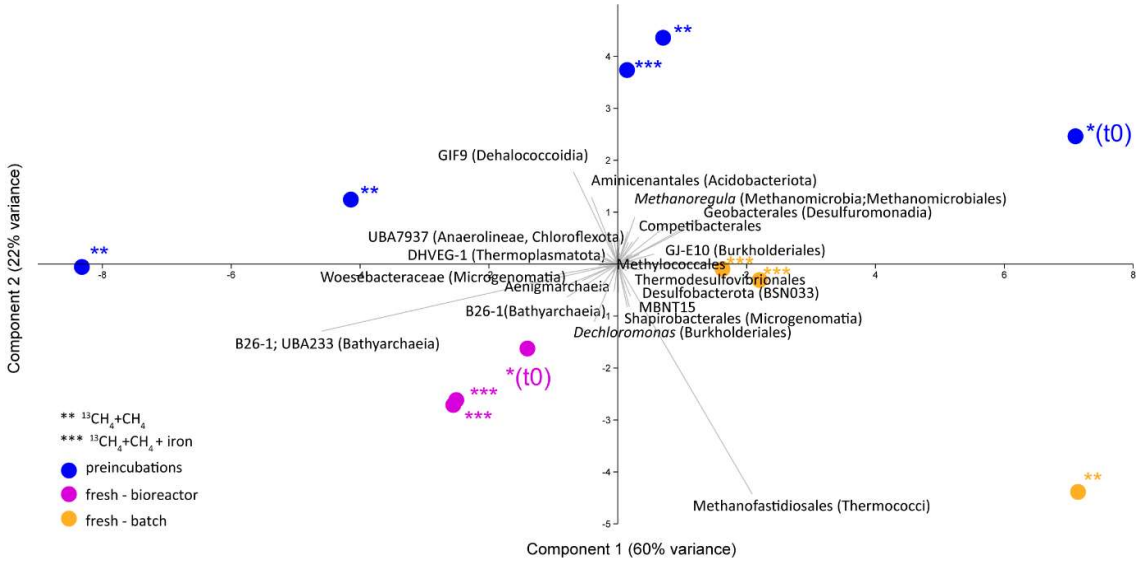

Figure 6: Principal component analysis comparing three types of samples: long-term pre-incubated slurries (blue – experiment A), semi-bioreactor (pink – experiment B) and fresh batch experiments (orange – experiment C). One asterisk represents t0, two asterisks denote methane-only treatments, three asterisks represent hematite treatment.

3.3 Lipid analysis

386 The $\delta^{13}C$ values of the archaeol-derived isoprenoid phytane in the long-term pre-incubated samples
387 were between -5 and -17‰ and thus showed a ^{13}C-enrichment between 15-27‰ relative to the original
388 sediment, indicative of methane-derived carbon assimilation by archaea (Table 3). This was less
389 pronounced for acyclic biphytane, dominantly derived from caldarchaeol, which showed a ^{13}C-
390 enrichment of 5-10‰. For bacterial-derived fatty acids, the shift in $\delta^{13}C$-values of up to 10‰ relative
391 to the original sediment was in a similar range but would have been expected to be much higher if
392 aerobic methanotrophs were active as was previously indicated by the extreme ^{13}C-enrichment of up to
393 1,650‰ observed in freshly incubated batch samples (Bar-Or et al., 2017).

394 Table 3: The $\delta^{13}C$ values (in ‰) of fatty acids and isoprenoid hydrocarbons from different experiments compared
395 to values obtained from the original sediment in the methanogenic zone.

			Fatty acids		Hydrocarbons	
Description	Temperature (°C)	Sampling (days)	$C_{16:1\omega9/8/7}$	$C_{16:1\omega5}$	Phytane	Biphytane
Pre-incubated slurry +$^{13}CH_4$+hematite	20	411	-40	-43	-17	-23
Pre-incubated slurry +$^{13}CH_4$ (bottle A)	20	411	-40	-43	-13	-24
Pre-incubated slurry +$^{13}CH_4$ (bottle B)	20	1227	-36	-41	-5	-38
[a] Fresh batch experiment+$^{13}CH_4$+hematite	20	470	610	1600	-14	-28
Semi-bioreactor+$^{13}CH_4$+hematite	16	382	n.d.	n.d.	n.d.	n.d.
Original sediment (28-30 cm)	14		-44	-51	-32	-33

[a] Bar-Or et al., 2017
n.d. – Not detected

396

397 # 4. Discussion

398 ## 4.1 AOM is maintained in long-term two-stage incubation experiments

399 Our previous porewater profiles of Lake Kinneret indicate that microbial sulfate reduction dominates
400 the anoxic hypolimnion and the surface sediments, while methanogenesis is confined to the sediments
401 below the sulfate boundary (Adler et al., 2011; Sivan et al., 2011; Bar-Or et al., 2015). The *in-situ*
402 geochemical and microbial diversity profiles, as well as geochemical and metagenomic analyses of
403 batch incubations with fresh sediments, provided evidence for Fe-AOM in the deep methanogenic zone
404 below 20 cm depth (Adler et al., 2011; Sivan et al., 2011; Bar-Or et al., 2015; Bar-Or et al., 2017; Elul
405 et al., 2021; Fig. 2). The profiles and the incubations showed an unexpected presence of aerobic
406 bacterial methanotrophs together with anaerobic microorganisms, such as methanogens and iron
407 reducers, in the anoxic sediments. They suggested that both *mcr* gene-bearing archaea and aerobic
408 bacterial methanotrophs mediate methane oxidation. In this study analyses of ^{13}C-DIC derived from
409 ^{13}C-labeled methane suggest that considerable AOM takes place also in the long-term incubations, even
410 after the two stages and the low abundance of the microbial populations. Below, we characterize this
411 AOM process in these incubation experiments.

412 ## 4.1 Potential electron acceptors for AOM in the long-term two-stage incubation experiments

The pre-incubated long-term incubations data show a sharp increase in the $\delta^{13}C_{DIC}$ values of both natural (methane-only) and hematite amendments in the two-stage incubations (Fig. 2). However, no difference in $\delta^{13}C_{DIC}$ between the two treatments was observed following the addition of hematite as the electron acceptor. This differs from the experiments B and C observations with fresh sediment, where the addition of hematite showed higher values than the methane-only treatment (Fig. 2; Bar-Or et al., 2017). This was particularly dramatic in the batch slurries (experiment C), but it was also significant in the semi-bioreactor (experiment B). We believe that the difference in the bioreactors would have been more pronounced if methane concentrations were higher, but it is still significant. The results suggest that either hematite lacks the potential to stimulate the AOM activity during long-term experiments or the presence of enough natural Fe(III) in the sediments to sustain the maximum potential of Fe-AOM.

Measurements of $\delta^{13}C_{DIC}$ show that additions of magnetite, amorphous iron, ferric iron from clays and manganese oxide in the two-stage incubations result in a less pronounced increase in the $\delta^{13}C_{DIC}$ values compared to the methane only controls (Figs. 2 and 3), reducing the AOM signal. One possible explanation is that these metal oxides may inhibit AOM, either directly or by a preference for organoclastic iron reduction over Fe-AOM, which adds isotopically light carbon from the organics rather than heavy carbon from the ^{13}C-labeled methane. Using mass-balance estimations in the methane-only treatments and the amorphous iron ones and considering the DIC concentrations and $\delta^{13}C_{DIC}$ values of the methane-only treatments at the beginning of the experiment (6 mM and 60‰, respectively) and the values at the end (6.5 mM and 360‰, respectively), about 0.5 mM of the DIC was added by AOM of methane with $\delta^{13}C$ of ~4000‰. The DIC and $\delta^{13}C_{DIC}$ values of the amorphous iron treatment at the beginning of the experiment were 5.4 mM and 60‰, respectively, and the values at the end were 6.1 mM and 120‰, respectively. Assuming the same $\delta^{13}C$ of the added methane of 4000‰ and $\delta^{13}C_{TOC}$ of -30‰ (Sivan et al., 2011), 0.1 mM of the DIC should derive from AOM and 0.6 mM from organoclastic metabolism. This means that adding amorphous iron to the system decreased the AOM activity and encouraged the oxidation of other organic compounds rather than methane. Intrinsic microbes, particularly the commonly detected ex-deltaproteobacterial lineages such as Geobacterales, may catalyze Fe(III) metal reduction, regardless of AOM. Manganese oxides are found in very low abundance in Lake Kinneret sediments (0.1 %, Table S1). Thus, their role in metal-AOM is likely minimal.

Sulfate concentrations in the methanogenic Lake Kinneret sediments are low (< 5 μM, Bar-Or et al., 2015; Elul et al., 2021). Sulfide concentrations have also been reported to be minor (<0.3 μM, Sivan et al., 2011). However, since pyrite and FeS precipitate in the top sediments, cryptic cycling via pyrite or FeS may replenish sulfate available for AOM (Bottrell et al., 2000). Na-molybdate addition to the two-stage slurries, including those amended with and without magnetite, did not change the $\delta^{13}C_{DIC}$ dynamics, which remained similar to those from before the inhibitor's addition (Fig. 3A). This is in line

with the fresh batch sediment slurries (Bar-Or et al., 2017) and hints that sulfate is not a potent electron acceptor for AOM in this environment. Furthermore, although sulfate-reducing bacteria were abundant, none of these reducers belonged to the known clades of ANME partners (Supplementary coverage table).

The nitrate and nitrite concentrations are undetectable in the porewater of Lake Kinneret sediments (Nüsslein et al., 2001; Sivan et al., 2011), but they may occur as an intermediate product of ammonium oxidation coupled to iron reduction. We thus assessed the role of nitrate and nitrite as electron acceptors in the two-stage slurries. The results indicate that the addition of nitrate delayed AOM and likely promoted denitrification. This is consistent with the fact that ANME-2d was not found. In the case of nitrite, even low concentrations appeared to delay the increase in $\delta^{13}C_{DIC}$ values, suggesting that organoclastic denitrification outcompetes AOM, and nitrite-AOM is not prominent in the two-stage incubations, despite the occurrence of Methylomirabilia (Figs. 3C, D).

Humic substances may promote AOM by continuously shuttling electrons to metal oxides (Valenzuela et al., 2019). Humic substances were not measured directly in Lake Kinneret sediments, but the DOC concentrations in porewater at the methanogenic depth were high (~1.5 mM, Adler et al., 2011), suggesting that they play a role in AOM. The addition of the synthetic humic analogs AQDS did not cause any enrichment in ^{13}C-DIC, but an increase of the dissolved Fe(II) concentrations compared to the methane-only treatments. This may be explained by AQDS acting as an electron shuttle in organoclastic iron reduction, producing isotopically light carbon that masks the AOM signal (Fig. 3E, Fig. S4). Yet, the natural humic substances may support AOM, as was suggested by Valenzuela et al. (2017). In our incubations, the natural humic substances promoted oxidation of organic matter and iron reduction at first, probably by shuttling electrons from organic compounds other than methane to natural iron oxides in the sediments (Figs. 3B and 4). Then, when the availability of the iron oxides or the organic matter decreased, humic substances likely facilitated AOM (Fig. 3B).

Overall, our long-term batch experiments, which included different electron acceptors, indicate that sulfate, nitrate, nitrite and Mn-oxides do not support AOM in Lake Kinneret methanogenic sediments. The potential electron acceptors are natural humic substrates with or without iron minerals that are abundant in the sediment and preferably react with methane rather than with other organics. The involvement of iron oxides in the AOM will be further explored after removing natural iron oxides from the sediments to simulate iron limitation.

4.2 Main microbial players in the long-term pre-incubated slurries

Methane oxidation in the pre-incubated Lake Kinneret sediments is likely mediated by either ANMEs or methanogens, as the addition of BES, a specific inhibitor for methanogens and ANME's mcrA genes, and acetylene immediately stopped the AOM, similarly to the killed bottles, and the BES addition to fresh sediment experiments (Bar-Or et a., 2017) (Fig. 5). Apart from methane-metabolizing organisms,

acetylene can inhibit nitrogen cycling, resulting in ethylene production (Oremland and Capone, 1988). This is not the case in our incubations, as no ethylene was produced. The increase in $\delta^{13}C$ values in phytane and biphytane (Table 3) also indicates active archaeal methanogens or ANMEs (Wegener et al., 2008; Kellermann et al., 2012; Kurth et al., 2019).

Using the isotopic composition of specific lipids and metagenomics, we identified a considerable abundance of aerobic methanotrophs and methylotrophs in the fresh sediments, but not in the pre-incubation slurries (Table 3, Fig. 6), suggesting a minor role of these lineages in the latter. The metagenomic data (Fig. 6, Supplementary coverage table) also indicate that Bathyarchaeia, which might be involved in methane metabolism (Evens et al., 2015), were enriched in the bioreactor incubations, yet their role in Lake Kineret AOM remains to be evaluated. ANME-1 are likely mediators of AOM in these sediments, although methane oxidation via the reverse methanogenesis is feasible for some methanogens in Lake Kinneret sediments (Elul et al., 2021). We also observed changes in abundance of bacterial degraders of organic matter and necromass: for example, GIF9 Dehalococcoidia, which can metabolize complex organics under methanogenic conditions (Cheng et al., 2019; Hug et al., 2013), were most abundant in long-term incubations (Fig. 6, Supplementary coverage table).

4.3 Mechanism of methane oxidation in the long-term incubations – AOM versus back flux

Our results indicate net methanogenesis in the two-stage incubation experiments with an average rate of 25 nmol gr^{-1} dry sediment day^{-1} (Table 2, Fig. S3 and Table S2), similar to fresh incubation experiments (Bar-Or et al., 2017), despite the overall increasing trend of $\delta^{13}C_{DIC}$ values resulting from potential methane turnover (Figs. 2 and 3). A likely explanation for both signals is an interplay between methane production and oxidation, with the latter triggered by reverse methanogenesis in bona fide ANMEs or some methanogens (Hallam et al., 2004; Timmers et al., 2017). Due to the overall production of methane and the lack of intensive stimulation of AOM by any electron acceptor, the significant increase in $\delta^{13}C_{DIC}$ values could theoretically result from carbon back flux during methanogenesis, which is feasible in environments close to thermodynamic equilibrium (Gropp et al., 2021). We used DIC mass balance calculations to determine whether back flux can be accounted for in the incubations. Based on equations 1 and 2, 3-8% of the ^{13}C-methane should be converted into DIC to reach the observed ^{13}C-enrichment. These estimates are orders of magnitude higher than the previously reported 0.001-0.3% values for methanogenesis back flux in cultures (Zehnder and Brock, 1979; Moran et al., 2005), and in the same range of 3.2 to 5.5% of back flux observed in ANME-enrichment cultures (Holler et al., 2011). In contrast, modeling approaches from AOM-dominated marine sediment samples and associated ANME enrichment cultures indicated the absence of net methanogenesis (Yoshinaga et al., 2014; Chuang et al., 2019; Meister et al., 2019; Wegener et al., 2021). Thus, it is unlikely that back flux alone can account for the methane-DIC conversion in Lake Kinneret sediments. Moreover, just back flux in marine methanogenic sediment with similar net methanogenesis rates and abundant methane-

metabolizing archaea did not yield any significant ^{13}C-enrichment in the DIC pool following sediment incubations (Sela-Adler et al., 2015; Amiel, 2018; Vigderovich et al., 2019; Yorshensky, 2019) (Table S3). Therefore, methanogenesis back flux alone seems less likely to sustain the observed DIC values than active AOM.

Conclusions

The geochemical and microbial profiles together with fresh sediment incubations showed evidence for Fe-AOM in the methanogenic zone of Lake Kinneret, which removes about 10-15% of the produced methane (Adler et al., 2011; Sivan et al., 2011). Anaerobic archaea appear to carry out methane turnover in these reduced sediments by reverse methanogenesis, but aerobic Methylococcales may be involved in methane oxidation, which is in line with other evidence of aerobic bacterial activity in the deep anoxic hypolimnion of lakes and their shallow sediments (Beck et al., 2013; Oswald et al., 2016; Martinez-Cruz et al., 2017; Cabrol et al., 2020). The simultaneous presence of aerobes and anaerobes in nature, even 20 meters below the thermocline and oxycline, may result from trace amounts of oxygen trapped in nano-niches or even in mineral layers (Wang et al., 2018), even if sensitive sensors do not detect them. This oxygen portion may not be removed by purging at the beginning of our experiments but is rather slowly used by the methanotrophs for their survival. However, after several incubation stages and intensive purging for a prolonged time, only archaea remained active and were involved in methane turnover, which was most likely coupled to the reduction of electron acceptors such as humic substances and iron.

Competing interests. The authors declare that they have no conflict of interest.

Acknowledgements

We would like to thank B. Sulimani and O. Tzabari from the Yigal Allon Kinneret Limnological Laboratory for their onboard technical assistance. We thank all of O. Sivan's lab members for their help during sampling, and especially to N. Lotem for the help with the mass balance calculations and discussions and to E. Eliani-Russak for her technical assistance. Many thanks to K. Hachmann from M. Elvert's lab for his help during lipid analysis and to J. Gropp for insightful discussions on the back flux. This work was supported by the ERC consolidator grant (818450) and the Israel Science Foundation (857-2016) of O. Sivan. Funding for M. Elvert was provided by the Deutsche Forschungsgemeinschaft (DFG) (49926684) and EXC 2077 (390741601). Funding for M. Rubin-Blum was provided by the Israel Science Foundation (913/19), the U.S.-Israel Binational Science Foundation (2019055) and Ministry of Science and Technology (1126), and H. Vigderovich was supported by the student fellowship of the Israeli water authority.

References

Adler, Michal, Eckert, W., & Sivan, O. (2011). Quantifying rates of methanogenesis and methanotrophy in Lake Kinneret sediments (Israel) using porewater profiles. *Limnology and Oceanography*, *56*(4), 1525–1535. https://doi.org/10.4319/lo.2011.56.4.1525

Aepfler, R. F., Bühring, S. I., & Elvert, M. (2019). Substrate characteristic bacterial fatty acid production based on amino acid assimilation and transformation in marine sediments. *FEMS Microbiology Ecology*, *95*(10), 1–15. https://doi.org/10.1093/femsec/fiz131

Amiel, N. (2018). *Authigenic magnetite in deep sediments.* MsC thesis, Ben Gurion University of the Negev.

Aromokeye, D. A., Kulkarni, A. C., Elvert, M., Wegener, G., Henkel, S., Coffinet, S., Eickhorst,T., Oni, O. E., Richter-Heitmann, T., Schnakenberg, A., Taubner, H., Wunder, L., Yin, X., Zhu, Q., Hinrichs, KU., Kasten, S., & Friedrich, M. W. (2020). Rates and Microbial Players of Iron-Driven Anaerobic Oxidation of Methane in Methanic Marine Sediments. *Frontiers in Microbiology*, *10*(January), 1–19. https://doi.org/10.3389/fmicb.2019.03041

Arshad, A., Speth, D. R., De Graaf, R. M., Op den Camp, H. J. M., Jetten, M. S. M., & Welte, C. U. (2015). A metagenomics-based metabolic model of nitrate-dependent anaerobic oxidation of methane by Methanoperedens-like archaea. *Frontiers in Microbiology*, *6*(DEC), 1–14. https://doi.org/10.3389/fmicb.2015.01423

Bai, Y. N., Wang, X. N., Wu, J., Lu, Y. Z., Fu, L., Zhang, F., Lau, TC., & Zeng, R. J. (2019). Humic substances as electron acceptors for anaerobic oxidation of methane driven by ANME-2d. *Water Research*, *164*, 114935. https://doi.org/10.1016/j.watres.2019.114935

Bankevich, A., Nurk, S., Antipov, D., Gurevich, A. a., Dvorkin, M., Kulikov, A. S., Lesin, V. M., Nicolenko, S. I., Pham, S., Prjibelski, A. D., Sirotkin, A. V., Vyahhi, N., Tesler, G., Aleksyev, A. M., & Pevzner, P. a. (2012). SPAdes: A New Genome Assembly Algorithm and Its Applications to Single-Cell Sequencing. *Journal of Computational Biology*, *19*(5), 455–477. https://doi.org/10.1089/cmb.2012.0021

Bar-Or, I., Ben-Dov, E., Kushmaro, A., Eckert, W., & Sivan, O. (2015). *Methane-related changes in prokaryotes along geochemical profiles in sediments of Lake Kinneret (Israel) Methane-related changes in prokaryotes along geochemical profiles in sediments of Lake Kinneret (Israel)*. (August). https://doi.org/10.5194/bg-12-2847-2015

Bar-Or, I., Elvert, M., Eckert, W., Kushmaro, A., Vigderovich, H., Zhu, Q., Ben-Dov, E., & Sivan, O. (2017). Iron-Coupled Anaerobic Oxidation of Methane Performed by a Mixed Bacterial-Archaeal Community Based on Poorly Reactive Minerals. *Environmental Science & Technology*, *51*, 12293–12301. https://doi.org/10.1021/acs.est.7b03126

Beal, E. J., House, C. H., & Orphan, V. J. (2009). Manganese-and Iron-Dependent Marine Methane Oxidation. *Science (New York, N.Y.)*, *325*(5937), 184–187. https://doi.org/10.1126/science.1169984

Beck, D. A. C., Kalyuzhnaya, M. G., Malfatti, S., Tringe, S. G., del Rio, T. G., Ivanova, N., Lidstorm, M. E., &

Chistoserdova, L. (2013). A metagenomic insight into freshwater methane-utilizing communities and evidence for cooperation between the Methylococcaceae and the Methylophilaceae. *PeerJ*, *2013*(1), 1–23. https://doi.org/10.7717/peerj.23

Biderre-Petit, C., Dugat-Bony, E., Mege, M., Parisot, N., Adrian, L., Moné, A., Denonfoux, J., Peyretaillade, E., Debroas. D., Boucher, D., Peyret, P. (2016). Distribution of Dehalococcoidia in the anaerobic deep water of a remote meromictic crater lake and detection of Dehalococcoidia-derived reductive dehalogenase homologous genes. *PLoS ONE*, *11*(1), 1–19. https://doi.org/10.1371/journal.pone.0145558

Boetius, A., Ravenschlag, K., Schubert, C. J., Rickert, D., Widdel, F., Gieseke, A., Amann, R., Jørgensen, B.B., Witte, U., & Pfannkuche, O. (2000). A marine microbial consortium apparently mediating AOM. *Nature*, *407*(October), 623–626.

Bottrell, S. H., Parkes, R. J., Cragg, B. A., & Raiswell, R. (2000): Isotopic evidence for anoxic pyrite oxidation and stimulation of bacterial sulphate reduction in marine sediments, *J. Geol. Soc. London*,157, 711–714. https://doi.org/10.1144/jgs.157.4.711.

Cabrol, L., Thalasso, F., Gandois, L., Sepulveda-Jauregui, A., Martinez-Cruz, K., Teisserenc, R., Tananaev, N., Tveit, A., Svenning, M. M., & Barret, M. (2020). Anaerobic oxidation of methane and associated microbiome in anoxic water of Northwestern Siberian lakes. *Science of the Total Environment*, *736*, 139588. https://doi.org/10.1016/j.scitotenv.2020.139588

Cheng, L., Shi, S. bao, Yang, L., Zhang, Y., Dolfing, J., Sun, Y. ge, Liu, L., Li, Q., Tu, B., Dai, L., Shi, Q., & Zhang, H. (2019). Preferential degradation of long-chain alkyl substituted hydrocarbons in heavy oil under methanogenic conditions. *Organic Geochemistry*, *138*. https://doi.org/10.1016/j.orggeochem.2019.103927

Chuang, P. C., Yang, T. F., Wallmann, K., Matsumoto, R., Hu, C. Y., Chen, H. W., Lin, S., Sun, CH., Li, HC., Wang, Y., & Dale, A. W. (2019). Carbon isotope exchange during anaerobic oxidation of methane (AOM) in sediments of the northeastern South China Sea. *Geochimica et Cosmochimica Acta*, *246*, 138–155. https://doi.org/10.1016/j.gca.2018.11.003

Conrad, R. (2009). The global methane cycle: Recent advances in understanding the microbial processes involved. *Environmental Microbiology Reports*, *1*(5), 285–292. https://doi.org/10.1111/j.1758-2229.2009.00038.x

Dershwitz, P., Bandow, N. L., Yang, J., Semrau, J. D., McEllistrem, M. T., Heinze, R. A., Fonseca, M., Ledesma, J. C., Jennett, J. R., DiSpirito, A. M., Athwal, N. S., Hargrove, M. S., Bobik, T. A., Zischka, H., & DiSpirito, A. A. (2021). Oxygen Generation via Water Splitting by a Novel Biogenic Metal Ion-Binding Compound. *Applied and Environmental Microbiology*, *87*(14), 1–14. https://doi.org/10.1128/aem.00286-21

Eckert, T. (2000). The Influence of Chemical Stratification in the Water Column on Sulfur and Iron Dynamics in Pore Waters and Sediments of Lake Kinneret, Israel. *M.Sc. Thesis,* University of Bayreuth, Germany.

Egger, M., Rasigraf, O., Sapart, C. J., Jilbert, T., Jetten, M. S. M., Röckmann, T., van der Veen, C., Bândă, N., Kartal, B., Ettwig, K. F., & Slomp, C. P. (2015). Iron-mediated anaerobic oxidation of methane in

brackish coastal sediments. *Environmental Science and Technology*, *49*(1), 277–283. https://doi.org/10.1021/es503663z

Elul, M., Rubin-Blum, M., Ronen, Z., Bar-Or, I., Eckert, W., & Sivan, O. (2021). Metagenomic insights into the metabolism of microbial communities that mediate iron and methane cycling in Lake Kinneret sediments. *Biogeosciences Discussions*, 1–24. https://doi.org/10.5194/bg-2020-329

Elvert, M., Boetius, A., Knittel, K., & Jørgensen, B. B. (2003). Characterization of specific membrane fatty acids as chemotaxonomic markers for sulfate-reducing bacteria involved in anaerobic oxidation of methane. *Geomicrobiology Journal*, *20*(4), 403–419. https://doi.org/10.1080/01490450303894

Ettwig, Katharina F, Butler, M. K., Le Paslier, D., Pelletier, E., Mangenot, S., Kuypers, M. M. M., Schreiber, F., Dutilh, B. E., Zedelius, J., de Beer, D. Gloerich, J., Wessels, H. J. C. T., van Alen, T., Luesken, F., Wu, M. L., van de Pas-Schoonen K. T., Op den Camp, H. J. M., Jansen-Megens, E. M., Francojs, KJ., Stunnenberg, H., Weissenbach, J., Jetten, M. S. M., & Strous, M. (2010). Nitrite-driven anaerobic methane oxidation by oxygenic bacteria. *Nature*, *464*(7288), 543–548. https://doi.org/10.1038/nature08883

Evans, P. N., Parks, D. H., Chadwick, G. L., Robbins, S, J., Orphan V. J., Golding, S. D., & Tyson, G. W. (2015). *Science*. 350(6259), 434-438. http://doi.org/ 10.1126/science.aac7745.

Fan, L., Dippold, M. A., Ge, T., Wu, J., Thiel, V., Kuzyakov, Y., & Dorodnikov, M. (2020). Anaerobic oxidation of methane in paddy soil: Role of electron acceptors and fertilization in mitigating CH4 fluxes. *Soil Biology and Biochemistry*, *141*, 107685. https://doi.org/10.1016/j.soilbio.2019.107685

Gropp, J., Iron, M. A., & Halevy, I. (2021). Theoretical estimates of equilibrium carbon and hydrogen isotope effects in microbial methane production and anaerobic oxidation of methane. *Geochimica et Cosmochimica Acta*, *295*, 237–264. https://doi.org/10.1016/j.gca.2020.10.018

Hadas, O., & Pinkas, R. (1995). Sulphate reduction in the hypolimnion and sediments of Lake Kinneret , Israel. *Freshwater Biology*, (33), 63–72.

Hallam, S. J., Putnam, N., Preston, C. M., Detter, J. C., Rokhsar, D., Richardson, P. H., & DeLong, E. F. (2004). Reverse methanogenesis: Testing the hypothesis with environmental genomics. *Science*, *305*(5689), 1457–1462. https://doi.org/10.1126/science.1100025

Hammer, Ø., Harper, D. A. T., & Ryan, P. D. (2001) Past: paleontological statistics software package for education and data analysis. *Paleontologia-Electronica*. 4 (1), 9.

Haroon, M. F., Hu, S., Shi, Y., Imelfort, M., Keller, J., Hugenholtz, P., Yuan, Z., & Tyson, G. W. (2013). Anaerobic oxidation of methane coupled to nitrate reduction in a novel archaeal lineage. *Nature*, *500*(7464), 567–570. https://doi.org/10.1038/nature12375

Hoehler, T. M., Alperin, M. J., Albert, D. B., & Martens, C. S. (1994). Field and laboratory, evidence for a methane-sulfate reducer consortium.pdf. *Global Biogeochemical Cycles*, *8*(4), 451–463.

Holler, T., Wegener, G., Niemann, H., Deusner, C., Ferdelman, T. G., Boetius, A., Brunner, B., & Widdel, F. (2011). Carbon and sulfur back flux during anaerobic microbial oxidation of methane and coupled sulfate

reduction. *Proceedings of the National Academy of Sciences of the United States of America*, *108*(52). https://doi.org/10.1073/pnas.1106032108

Holmkvist, L., Ferdelman, T. G., & Jørgensen, B. B. (2011). A cryptic sulfur cycle driven by iron in the methane zone of marine sediment (Aarhus Bay, Denmark). *Geochimica et Cosmochimica Acta*, *75*(12), 3581–3599. https://doi.org/10.1016/j.gca.2011.03.033

Hug, L. A., Castelle, C. J., Wrighton, K. C., Thomas, B. C., Sharon, I., Frischkorn, K. R., Williams, K. H., Tringe, S. G., & Banfield, J. F. (2013). Community genomic analyses constrain the distribution of metabolic traits across the Chloroflexi phylum and indicate roles in sediment carbon cycling. *Microbiome*, *1*(1), 1–17. https://doi.org/10.1186/2049-2618-1-22

Kang, D. D., Li, F., Kirton, E., Thomas, A., Egan, R., An, H., & Wang, Z. (2019). MetaBAT 2: An adaptive binning algorithm for robust and efficient genome reconstruction from metagenome assemblies. *PeerJ*, *2019*(7), 1–13. https://doi.org/10.7717/peerj.7359

Kellermann, M. Y., Wegener, G., Elvert, M., Yoshinaga, M. Y., Lin, Y. S., Holler, T., Mollar, P. X., Knittel K., & Hinrichs, K. U. (2012). Autotrophy as a predominant mode of carbon fixation in anaerobic methane-oxidizing microbial communities. *Proceedings of the National Academy of Sciences of the USA* 109(47), 19321-19326. doi:10.1073/pnas.1208795109.

Kits, K. D., Klotz, M. G., & Stein, L. Y. (2015). Methane oxidation coupled to nitrate reduction under hypoxia by the Gammaproteobacterium Methylomonas denitrificans, sp. nov. type strain FJG1. *Environmental Microbiology*, *17*(9), 3219–3232. https://doi.org/10.1111/1462-2920.12772

Knittel, K., & Boetius, A. (2009). Anaerobic oxidation of methane: Progress with an unknown process. *Annual Review of Microbiology*, *63*, 311–334. https://doi.org/10.1146/annurev.micro.61.080706.093130

Kurth, J.M., Nadine T Smit, Stefanie Berger, Stefan Schouten, Mike S M Jetten, Cornelia U Welte, Anaerobic methanotrophic archaea of the ANME-2d clade feature lipid composition that differs from other ANME archaea, FEMS Microbiology Ecology, Volume 95, Issue 7, July 2019, fiz082.

Li, X., Hou, L., Liu, M., Zheng, Y., Yin, G., Lin, X., Cheng, L., Li, Y., & Hu, X. (2015). Evidence of Nitrogen Loss from Anaerobic Ammonium Oxidation Coupled with Ferric Iron Reduction in an Intertidal Wetland. *Environmental Science and Technology*, *49*(19), 11560–11568. https://doi.org/10.1021/acs.est.5b03419

Lin, Y. S., Lipp, J. S., Yoshinaga, M. Y., Lin, S. H., Elvert, M., & Hinrichs, K. U. (2010). Intramolecular stable carbon isotopic analysis of archaeal glycosyl tetraether lipids. *Rapid Communications in Mass Spectrometry*, *24*(19), 2817–2826. https://doi.org/10.1002/rcm.4707

Lovley, D. R., & Klug, M. J. (1983). Sulfate reducers can outcompete methanogens at freshwater sulfate concentrations. *Applied and Environmental Microbiology*, *45*(1), 187–192. https://doi.org/10.1128/aem.45.1.187-192.1983

Luo, J. H., Chen, H., Hu, S., Cai, C., Yuan, Z., & Guo, J. (2018). Microbial Selenate Reduction Driven by a Denitrifying Anaerobic Methane Oxidation Biofilm. *Environmental Science and Technology*, *52*(7),

695 4006–4012. https://doi.org/10.1021/acs.est.7b05046

696 Martinez-cruz, K., Leewis, M., Charold, I., Sepulveda-jauregui, A., Walter, K., Thalasso, F., & Beth, M. (2017).
697 Science of the Total Environment Anaerobic oxidation of methane by aerobic methanotrophs in sub-
698 Arctic lake sediments. *Science of the Total Environment*, *607–608*, 23–31.
699 https://doi.org/10.1016/j.scitotenv.2017.06.187

700 Meador, T. B., Gagen, E. J., Loscar, M. E., Goldhammer, T., Yoshinaga, M. Y., Wendt, J., Thomm, M., &
701 Hinrichs, K. U. (2014). Thermococcus kodakarensis modulates its polar membrane lipids and elemental
702 composition according to growth stage and phosphate availability. *Frontiers in Microbiology*, *5*(JAN), 1–
703 13. https://doi.org/10.3389/fmicb.2014.00010

704 Meister, P., Liu, B., Khalili, A., Böttcher, M. E., & Jørgensen, B. B. (2019). Factors controlling the carbon
705 isotope composition of dissolved inorganic carbon and methane in marine porewater: An evaluation by
706 reaction-transport modelling. *Journal of Marine Systems*, *200*(August), 103227.
707 https://doi.org/10.1016/j.jmarsys.2019.103227

708 Moran, J. J., House, C. H., Freeman, K. H., & Ferry, J. G. (2005). Trace methane oxidation studied in several
709 Euryarchaeota under diverse conditions. *Archaea*, *1*(5), 303–309. https://doi.org/10.1155/2005/650670

710 Mosrovaya, A., Wind-Hansen, M., Rousteau, P., Bristow, L. A., & Thamdrup, B. (2021) Sulfate- and iron-
711 dependent anaerobic methane oxidation occuring side-by-side in freshwater lake sediments. *Limnology*
712 *and Oceanography*. https://doi.org/10.1002/lno.11988

713 Nollet, L., Demeyer, D., & Verstraete, W. (1997). Effect of 2-bromoethanesulfonic acid and Peptostreptococcus
714 productus ATCC 35244 addition on stimulation of reductive acetogenesis in the ruminal ecosystem by
715 selective inhibition of methanogenesis. *Applied and Environmental Microbiology*, *63*(1), 194–200.
716 https://doi.org/10.1128/aem.63.1.194-200.1997

717 Nurk, S., Bankevich, A., & Antipov, D. (2013). Assembling genomes and mini-metagenomes from highly
718 chimeric reads. *Research in Computational Molecular Biology*, 158–170. https://doi.org/10.1007/978-3-
719 642-37195-0

720 Nüsslein, B., Chin, K. J., Eckert, W., & Conrad, R. (2001). Evidence for anaerobic syntrophic acetate oxidation
721 during methane production in the profundal sediment of subtropical Lake Kinneret (Israel). *Environmental*
722 *Microbiology*, *3*(7), 460–470. https://doi.org/10.1046/j.1462-2920.2001.00215.x

723 Orembland, R. S., & Capone, D. G. (1988). *Use of "Specific" Inhibitors in Biogeochemistry and Microbial*
724 *Ecology* (Vol. 10). https://doi.org/10.2307/4514

725 Orphan, V. J., House, C. H., & Hinrichs, K. (2001). Methane-Consuming Archaea Revealed by Directly
726 Coupled Isotopic and Phylogenetic Analysis. *Science*, *293*(July), 484–488.
727 https://doi.org/10.1126/science.1061338

728 Oswald, K., Milucka, J., Brand, A., Hach, P., Littmann, S., Wehrli, B., Albersten, M., Daims, H., Wagner, M.,
729 Kuypers, M. M. M., Schubert, C. J., & Milucka, J. (2016). Aerobic gammaproteobacterial methanotrophs

mitigate methane emissions from oxic and anoxic lake waters. *Limnology and Oceanography*, *61*, S101–S118. https://doi.org/10.1002/lno.10312

Parks, D. H., Chuvochina, M., Rinke, C., Mussig, A. J., Chaumeil, P-A., & Hugenholtz, P. (2021) GTDB: an ongoing census of bacterial and archaeal diversity through a phylogenetically consistent, rank normalized and complete genome-based taxonomy. *Nucleic Acids Research, 202, 1-10.* http://doi.org/10.1093/nar/gkab776

Raghoebarsing, A. A., Pol, A., Van De Pas-Schoonen, K. T., Smolders, A. J. P., Ettwig, K. F., Rijpstra, W. I. C., Schouten, S., Sinninghe Damsté, J. S., Op den Camp, H. J. M., Jetten, M. S. M., & Strous, M. (2006). A microbial consortium couples anaerobic methane oxidation to denitrification. *Nature*, *440*(7086), 918–921. https://doi.org/10.1038/nature04617

Reeburgh, W. S. (2007). Oceanic Methane Biogeochemistry. *ChemInform*, *38*(20), 486–513. https://doi.org/10.1002/chin.200720267

Saunois, M., Stavert, A. R., Poulter, B., Bousquet, P., Canadell, J. G., Jackson, R. B., Raymond, P. A., Dlugokencky, E. J., Houweling, S., Patra, P. K., Ciais, P., Arora, V. K., Bastviken, D., Bergamaschi, P., Blake, D. R., Brailsford, G., Bruhwiler, L., Carlson, K. M., Carrol, M., Castaldi, S., Chandra, N., Crevoisier, C., Crill, P. M., Covey, K., Curry, C. L., Etiope, G., Frankenberg, C., Gedney, N., Hegglin, M. I., Höglund-Isaksson, L., Hugelius, G., Ishizawa, M., Ito, A., Janssens-Maenhout, G., Jensen, K. M., Joos, F., Kleinen, T., Krummel, P. B., Langenfelds, R. L., Laruelle, G. G., Liu, L., Machida, T., Maksyutov, S., McDonald, K. C., McNorton, J., Miller, P. A., Melton, J. R., Morino, I., Müller, J., Murguia-Flores, F., Naik, V., Niwa, Y., Noce, S., O'Doherty, S., Parker, R. J., Peng, C., Peng, S., Peters, G. P., Prigent, C., Prinn, R., Ramonet, M., Regnier, P., Riley, W. J., Rosentreter, J. A., Segers, A., Simpson, I. J., Shi, H., Smith, S. J., Steele, L. P., Thornton, B. F., Tian, H., Tohjima, Y., Tubiello, F. N., Tsuruta, A., Viovy, N., Voulgarakis, A., Weber, T. S., van Weele, M., van der Werf, G. R., Weiss, R. F., Worthy, D., Wunch, D., Yin, Y., Yoshida, Y., Zhang, W., Zhang, Z., Zhao, Y., Zheng, B., Zhu, Q., Zhu, Q., and Zhuang, Q.: The Global Methane Budget 2000–2017, Earth Syst. Sci. Data, 12, 1561–1623, https://doi.org/10.5194/essd-12-1561-2020, 2020.

Scheller, S., Yu, H., Chadwick, G. L., McGlynn, S. E., & Orphan, V. J. (2016). Artificial electron acceptors decouple archaeal methane oxidation from sulfate reduction. *Science*, *351*(6274), 1754–1756. https://doi.org/10.1126/science.aad7154

Segarra, K. E. a, Comerford, C., Slaughter, J., & Joye, S. B. (2013). Impact of electron acceptor availability on the anaerobic oxidation of methane in coastal freshwater and brackish wetland sediments. *Geochimica et Cosmochimica Acta*, *115*, 15–30. https://doi.org/10.1016/j.gca.2013.03.029

Sela-Adler, M., Herut, B., Bar-Or, I., Antler, G., Eliani-Russak, E., Levy, E., Makovsky, Y., & Sivan, O. (2015). Geochemical evidence for biogenic methane production and consumption in the shallow sediments of the SE Mediterranean shelf (Israel). *Continental Shelf Research*, *101*, 117–124. https://doi.org/10.1016/j.csr.2015.04.001

Serruya, C. (1971). Lake Kinneret: the nutrient chemistry of the Sediments. *Limnology and Oceanography*,

16(May), 510–521.

Shuai, W., & Jaffé, P. R. (2019). Anaerobic ammonium oxidation coupled to iron reduction in constructed wetland mesocosms. *Science of the Total Environment*, *648*, 984–992. https://doi.org/10.1016/j.scitotenv.2018.08.189

Sieber, C. M. K., Probst, A. J., Sharrar, A., Thomas, B. C., Hess, M., Tringe, S. G., & Banfield, J. F. (2018). Recovery of genomes from metagenomes via a dereplication, aggregation and scoring strategy. *Nature Microbiology*, *3*(7), 836–843. https://doi.org/10.1038/s41564-018-0171-1

Sivan, O, Adler, M., Pearson, A., Gelman, F., Bar-Or, I., John, S. G., & Eckert, W. (2011). Geochemical evidence for iron-mediated anaerobic oxidation of methane. *Limnology and Oceanography*, *56*(4), 1536–1544.

Sivan, O., Antler, G., Turchyn, A. V., Marlow, J. J., & Orphan, V. J., (2014). Iron oxides stimulate sulfate-driven anaerobic methane oxidation in seeps. PNAS. 111, E4139-E4147. http://doi.org/10.1073/pnas.1412269111

Sivan, O., Shusta, S., & Valentine, D. L. (2016). Methanogens rapidly transition from methane production to iron reduction. *Geobiology*, 190–203. https://doi.org/10.1111/gbi.12172

Stookey, L. L. (1970). Ferrozine-a new spectrophotometric reagent for iron. *Analytical Chemistry*, *42*(7), 779–781. https://doi.org/10.1021/ac60289a016

Sturt, H. F., Summons, R. E., Smith, K., Elvert, M., & Hinrichs, K. U. (2004). Intact polar membrane lipids in prokaryotes and sediments deciphered by high-performance liquid chromatography/electrospray ionization multistage mass spectrometry - New biomarkers for biogeochemistry and microbial ecology. *Rapid Communications in Mass Spectrometry*, *18*(6), 617–628. https://doi.org/10.1002/rcm.1378

Su, G., Zopfi, J., Yao, H., Steinle, L., Niemann, H., & Lehmann, M. F. (2020). Manganese/iron-supported sulfate-dependent anaerobic oxidation of methane by archaea in lake sediments. *Limnology and Oceanography*, *65*(4), 863–875. https://doi.org/10.1002/lno.11354

Tamames, J., & Puente-Sánchez, F. (2019). SqueezeMeta, A Highly Portable, Fully Automatic Metagenomic Analysis Pipeline. *Frontiers in Microbiology*, *9*. https://doi.org/10.3389/fmicb.2018.03349

Timmers, P. H. A., Welte, C. U., Koehorst, J. J., Plugge, C. M., Jetten, M. S. M., & Stams, A. J. M. (2017). Reverse Methanogenesis and Respiration in Methanotrophic Archaea. *Archaea*, *2017*(Figure 1). https://doi.org/10.1155/2017/1654237

Treude, T., Krause, S., Maltby, J., Dale, A. W., Coffin, R., & Hamdan, L. J. (2014). Sulfate reduction and methane oxidation activity below the sulfate-methane transition zone in Alaskan Beaufort Sea continental margin sediments: Implications for deep sulfur cycling. *Geochimica et Cosmochimica Acta*, *144*, 217–237. https://doi.org/10.1016/j.gca.2014.08.018

Treude, T., Niggemann, J., Kallmeyer, J., Wintersteller, P., Schubert, C. J., Boetius, A., & Jørgensen, B. B. (2005). Anaerobic oxidation of methane and sulfate reduction along the Chilean continental margin.

802 *Geochimica et Cosmochimica Acta*, *69*(11), 2767–2779. https://doi.org/10.1016/j.gca.2005.01.002

803 Valenzuela, E. I., Avendaño, K. A., Balagurusamy, N., Arriaga, S., Nieto-Delgado, C., Thalasso, F., &
804 Cervantes, F. J. (2019). Electron shuttling mediated by humic substances fuels anaerobic methane
805 oxidation and carbon burial in wetland sediments. *Science of the Total Environment*, *650*, 2674–2684.
806 https://doi.org/10.1016/j.scitotenv.2018.09.388

807 Valenzuela, E. I., Prieto-Davó, A., López-Lozano, N. E., Hernández-Eligio, A., Vega-Alvarado, L., Juárez, K.,
808 García-González, A. S., López, M. G., & Cervantes, F. J. (2017). Anaerobic methane oxidation driven by
809 microbial reduction of natural organic matter in a tropical wetland. *Applied and Environmental*
810 *Microbiology*, *83*(11), 1–15. https://doi.org/10.1128/AEM.00645-17

811 Vigderovich, H., Liang, L., Herut, B., Wang, F., Wurgaft, E., Rubin-Blum, M., & Sivan, O. (2019). Evidence
812 for microbial iron reduction in the methanogenic sediments of the oligotrophic SE Mediterranean
813 continental shelf. *Biogeosciences Discussions*, 1–25. https://doi.org/10.5194/bg-2019-21

814 Wang, L., Miao, X., Ali, J., Lyu, T., & Pan, G. (2018). Quantification of Oxygen Nanobubbles in Particulate
815 Matters and Potential Applications in Remediation of Anaerobic Environment. *ACS Omega*, *3*(9), 10624–
816 10630. https://doi.org/10.1021/acsomega.8b00784

817 Wegener G, Niemann H, Elvert M, Hinrichs K-U, Boetius A (2008). Assimilation of methane and inorganic
818 carbon by microbial communities mediating the anaerobic oxidation of methane. Environmental
819 Microbiology 10(9), 2287-2298. doi: 10.1111/j.1462-2920.2008.01653.x.

820 Wegener, G., Gropp, J., Taubner, H., Halevy, I., & Elvert, M. (2021). Sulfate-dependent reversibility of
821 intracellular reactions explains the opposing isotope effects in the anaerobic oxidation of methane. *Science*
822 *Advances*, *7*(19), 1–14. https://doi.org/10.1126/sciadv.abe4939

823 Wu, Y.W., Tang, Y.-H., Tringe, S. G., Simmons, B. A., & Singer, S. W. (2014). MaxBin: an automated binning
824 method to recover individual genomes from metagenomes using. *Microbiome*, *2*(26), 4904–4909.
825 Retrieved from https://microbiomejournal.biomedcentral.com/articles/10.1186/2049-2618-2-26

826 Wuebbles, D. J., & Hayhoe, K. (2002). Atmospheric methane and global change. *Earth-Science Reviews*, *57*(3–
827 4), 177–210. https://doi.org/10.1016/S0012-8252(01)00062-9

828 Yorshansky, O. (2019). *Iron Reduction in Deep Marine Sediments of the Eastern Mediterranean Continental*
829 *Shelf and the Yarqon Estuary*. MsC thesis, Ben Gurion University of the Negev.

830 Yoshinaga, M. Y., Holler, T., Goldhammer, T., Wegener, G., Pohlman, J. W., Brunner, B., Kuypers, M. M. M.,
831 Hinrichs, K. U., & Elvert, M. (2014). Carbon isotope equilibration during sulphate-limited anaerobic
832 oxidation of methane. *Nature Geoscience*, *7*(3), 190–194. https://doi.org/10.1038/ngeo2069

833 Zehnder, a J., & Brock, T. D. (1979). Methane formation and methane oxidation by methanogenic bacteria.
834 *Journal of Bacteriology*, *137*(1), 420–432.

835 Zhang, X., Xia, J., Pu, J., Cai, C., Tyson, G. W., Yuan, Z., & Hu, S. (2019). Biochar-Mediated Anaerobic
836 Oxidation of Methane. *Environmental Science and Technology*, *53*(12), 6660–6668.

https://doi.org/10.1021/acs.est.9b01345

Zheng, Y., Wang, H., Liu, Y., Zhu, B., Li, J., Yang, Y., Qin, W., Chen, L., Wu, X., Chistoserdova, L., & Zhao, F. (2020). Methane-Dependent Mineral Reduction by Aerobic Methanotrophs under Hypoxia. *Environmental Science and Technology Letters*, *7*(8), 606–612. https://doi.org/10.1021/acs.estlett.0c00436